Accepted Manuscript

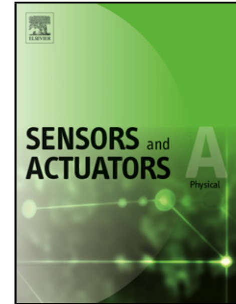

Title: An Investigation into the Mechanical Behavior of Multi-Input and Multi-Output MEMS Resonators

Authors: N. Alcheikh, S.A. Tella, M.I. Younis

PII: S0924-4247(18)30464-3
DOI: https://doi.org/10.1016/j.sna.2018.07.036
Reference: SNA 10901

To appear in: *Sensors and Actuators A*

Received date: 15-3-2018
Revised date: 12-6-2018
Accepted date: 17-7-2018

Please cite this article as: Alcheikh N, Tella SA, Younis MI, An Investigation into the Mechanical Behavior of Multi- Input and Multi-Output MEMS Resonators, *Sensors and Actuators: A. Physical* (2018), https://doi.org/10.1016/j.sna.2018.07.036

This is a PDF file of an unedited manuscript that has been accepted for publication. As a service to our customers we are providing this early version of the manuscript. The manuscript will undergo copyediting, typesetting, and review of the resulting proof before it is published in its final form. Please note that during the production process errors may be discovered which could affect the content, and all legal disclaimers that apply to the journal pertain.

ACCEPTED MANUSCRIPT

An Investigation into the Mechanical Behavior of Multi- Input and Multi-Output MEMS Resonators

N. Alcheikh, [1] S.A. Tella, [1] and M. I. Younis[1, 2,a]

[1]*Physical Science and Engineering Division, King Abdullah University of Science and Technology, Thuwal, 23955-6900, Saudi Arabia*

[2]*Department of Mechanical Engineering, State University of New York, Binghamton, NY 13902, USA*

ACCEPTED MANUSCRIPT

[a] Corresponding author Electronic mail: Mohammad.Younis@kaust.edu.sa

ACCEPTED MANUSCRIPT

Highlights

- We showed MEMS resonators with multiple electrical input and output possibilities.
- Resonators have been designed as in-plane arch clamped-guided microbeam attached to another T-shape beam from the side
- The devices provide an electrostatic and electrothermal tuning capability.
- Through theoretical and experimental investigations, we examined different ways of both sensing and actuation of two mechanically coupled resonators.
- We experimentally demonstrated that, this configuration operation depending on the actuation ways and the combination of the logic inputs and the two logic outputs allows the realization of complex logic operations, such as a 1:2 DEMUX.

ABSTRACT

We investigate theoretically and experimentally the mechanical behavior of Micro electromechanical systems MEMS resonators with multiple input (actuation) and output (detection) methods. The devices are based on a compound resonator consisting of an in-plane clamped-guided arch beam that is mechanically coupled from its guided side to another T-shaped resonant beam. Tensile and compressive bi-directional electrostatic axial forces are induced on the T-shaped resonator, which modulate the stiffness of both the arch and the T-shaped beams resonators, thereby changing their resonance frequencies to lower or higher values. At the coupling point of the two resonators, additional two flexure beams are attached, which provide another electrothermal tuning capability. The electrothermal actuators can be configured in various ways to adjust, as desired, the mechanical stiffness of the resonators; thereby controlling their resonance frequency. Therefore, this structure offers various electrothermal and electrostatic actuation and read-out possibilities, which can lead to complex device functionalities based on multiple inputs and outputs. As an example, we experimentally demonstrate an electromechanical resonant 1:2 DEMUX logic element. The logic operation is based on the linear frequency modulation. This study demonstrates that with such compound MEMS resonators, it is possible to build more complex logic functionalities.

ACCEPTED MANUSCRIPT

1. Introduction

Microelectromechanical systems (MEMS) resonators based on axially actuated microbeams have been investigated widely for many applications, such as pressure sensors [1-2], flow sensors [3], gas sensors [4], filters [5], memory elements [6-7], logic gaits [8], and accelerometers [9]. The implementation of MEMS as platforms for sensors has seen steady growth due to their small mass, low cost, high sensitivity and resolution, energy efficiency, and reliability [11-12]. In addition, these MEMS resonators have attracted major attention as an essential element for logic circuits, mostly due to the compatibility with electronic circuits, low power cost, dynamic mode of operation, and run time re-programmability.

Many of these applications are based on a doubly-clamped beam and widely use the electrothermal and electrostatic actuation to tune its resonance frequency [12-21]. Kessler et al. [3] showed a flow sensor based on the deflection monitoring of a microbeam buckled by the compressive thermal stress due to electrothermal Joule's heating. Bouchaala et al. [4] demonstrated a smart resonant mass sensor combining both sensing and actuation on the same device based on a single electrostatically actuated microbeam. Hajjaj et al. [1] proposed an alternative pressure sensor that offers the flexibility of being scalable to small or large sizes, based on the cooling effect of the air surrounding an electrothermally heated clamped-clamped beam resonator. Halg [22] demonstrated an integrated nonvolatile memory based on the bi-stable states of a micromechanical beam. In [23], several basic 2-bit and 3-bit logic operations have been demonstrated using an electrothermally actuated arch resonator.

To add more functionality to sensors and actuators, allow multi-frequency and multi-modal excitations, and to develop more complex and deep logic circuits, new designs of more complex resonators other than the traditional simple structures, such as beams and plates, are needed. Toward this goal, we demonstrate the design and testing of a MEMS resonator with multiple actuation inputs and multiple ports outputs. The resonator can be actuated through both electrostatic and electrothermal voltages and its output response can be read through several sensing electrodes.

In a recent work [24], we investigated experimentally and theoretically the ability to tune stiffness and frequency of a clamped-guided resonator using tensile and compressive axial forces generated from a bi-directional electrostatic actuator. In [7], we used this axial tuning to demonstrate reconfigurable logic and random access memory devices. The potential of such a device to be implemented as multiple-input and multiple-output compound resonator through using two resonating structures on the same device and through electrostatic and electrothermal actuations have not yet explored. This works aims to explore this concept.

In this paper, we investigate theoretically and experimentally different ways of both sensing and actuation on a single device made up of two mechanically coupled resonators. One resonator is an electrostatically excited in-plane clamped-guided arch microbeam. The other resonator is a T-shaped one, which is also provided with two side electrodes to apply bi-directional electrostatic actuation. Both resonators are coupled mechanically; and are attached at the point of coupling to two flexure beams that provide additional electrothermal actuations. Therefore, this

ACCEPTED MANUSCRIPT

structure offers various possibilities to control stiffness, and hence, leads to various possible inputs and outputs. This device can be used in applications requiring multi-inputs and multi-outputs.

In recent years, significant research has focused on the development of logic and memory devices based on MEMS resonators [25-26]. Although there have been successful demonstrations of fundamental logic gates, the realization of complex combinational logic gates has posed a great challenge. Yao et al. [27] demonstrated both logic and memory unit from a single MEMS resonator. Mahboob et al. [25] showed the capability of a single electromechanical resonator to perform logic functions in parallel and multibit complex logic. Hafiz et al. [28] demonstrated a 2:1 MUX, logic element, based on electrothermal frequency tuning of cascaded multiple arch resonators. However, cascading multiple MEMS resonators to perform complex logic operations introduces major practical challenges [29]. Despite advances in this area of research, constructing complex logic functions such as 1:2 DEMUX based on a single structure has not been reported yet.

In this work, we experimentally demonstrate the capability of the proposed device to realize a 1:2 DEMUX, an essential complex logic element, based on the electrostatic and electrothermal frequency tuning.

2. Background design and device principle

As shown in Fig. 1, the structure is composed of an in-plane arch microbeam, Fig. 1(a), which is clamped at one end and axially guided on the other end, two flexures beams, and T-shaped beam (Fig. 1(b)). Both arch and T-shaped beams represent two resonating structures. They both are sandwiched between electrodes from two sides. These electrodes can be used for electrostatic actuation (inputs) and also for sensing (outputs). Several ways can be used to control the stiffness of the two resonators: the arch beam and the T-shaped beam. Since the arch beam is mechanically attached to the T-shaped beam, the stiffness variations in both beams can affect their static and dynamic behavior. The arch beam is excited electrostatically by a DC polarization V_{DC} on the lower electrode, which causes an axial displacement u at the guided side, point "N" in Fig. 1(a), and leads to decreasing on its elastic stiffness and its first resonance frequency. When actuating the T-shaped beam, on the other hand, by applying an actuation voltage V_T (V_C) between the tensile (compressive) electrode and its mass, an axial displacement u is created at "N" (Fig. 1(b)), generating an axial tensile (compressive) force on the arch beam, thereby controlling stiffness and frequencies [24].

The resonance frequency of the T-shaped beam in the in-plane rotation mode can increase or decrease depending on the arch beam stiffness. The two flexure beams have been added to avoid the high rotation stiffness of the structure in the out-of-plane. Additionally, these beams can be electrothermally actuated, by passing a current through them. There are two actuation pads on the flexure beams labeled (A and B), which offer two ways of electrical connections, and hence electrothermal actuation combinations. Therefore, two cases are investigated in this paper: BV$^-$(A (V^+) - B (V^-) - D(G)), and BV$^+$(A (V^+) - B (V^+)- D(G)). Schematics of the current distribution for the two cases are shown in Figs. 1 (c-d). When these flexure beams are powered, their elastic stiffness change depending on the applied voltage and the amount of the current passing through the microbeam. Additionally, the pads of the flexure beams add another input to control the curvature and stiffness of arch beam and the T-shaped

ACCEPTED MANUSCRIPT

beam. Therefore, this structure offers various possibilities to control stiffness, and hence, leads to various possible inputs. As shown in Fig. 1, four electrostatic electrodes and two electrothermal pads labeled on the flexure beams can be used as inputs. Since the device is composed of two resonators (the arch beam and the T-shaped beam) where they can locally oscillate with minimum vibration effect on each other, the structure offers also various possible outputs.

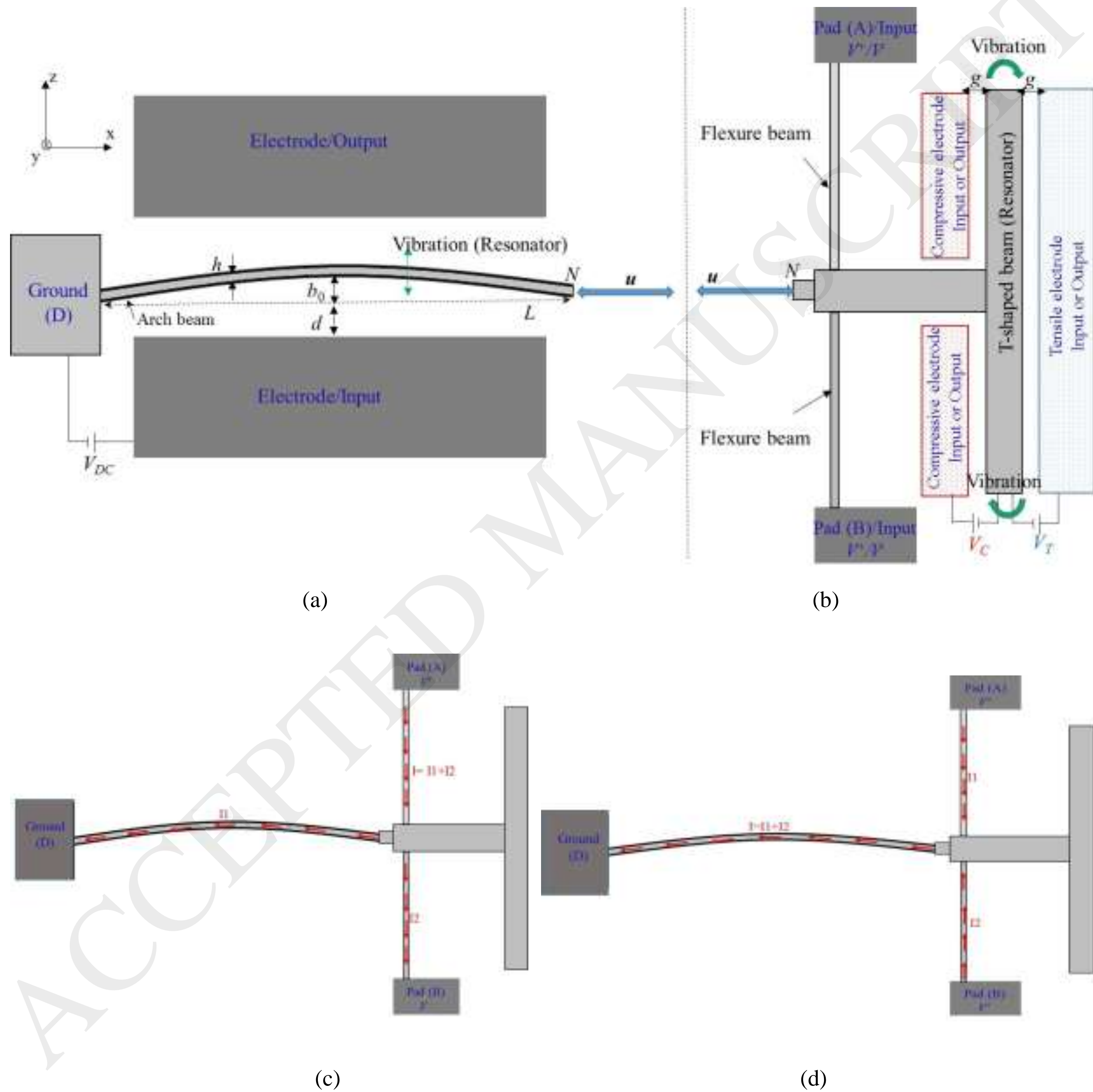

Fig. 1. A schematic of the device. The device consists of two resonators, (a) a fixed-guided microbeam and (b) a beam in T-shaped connected to two flexure beams. The arch beam can be actuated electrostatically (V_{DC}) or electrothermally from the flexure beams (BV$^-$ (A (V^+)-B (V^-)-D(G) or BV$^+$(A (V^+)-B (V^+)-D (G))). Schematics of the current distribution for (c) BV$^-$and (d) BV$^+$. The T-shaped beam can be actuated electrostatically by compressive load (V_C) or tensile load (V_T), or electrothermally

ACCEPTED MANUSCRIPT

ACCEPTED MANUSCRIPT

from the flexure beams. Note here that the arch beam vibrates in the bending mode while the T-shaped beam vibrates as a rigid body in the rotational mode, where the flexure beams provide torsional stiffness.

The structure is fabricated from a highly conductive silicon device layer of silicon-on-insulator (SOI) wafer from MEMSCAP [24]. The arch beam has 600 µm in length (L), 1.7 µm in width (h), 2.6 µm in initial rise (b_0), and 25µm in thickness. The gap between the actuated electrode and the clamped end of the arch beam (T-shaped beam) is 8 µm (2 µm). The length and the width of the T-shaped beam are 1000 µm and 35 µm, respectively. The flexure beams have 460 µm length, 10 µm width, and 25 µm in thickness.

3. Theoretical results and discussions

The inset schematics in Fig.2 (a-b), show, respectively, the mode in which the local motion of the arch beam and the local motion of T-shaped beam dominate. The frequency responses of these two dominating modes will be studied theoretically and experimentally.

Finite element models (FEM) of the device were developed with the software COMSOL to design, simulate, and investigate its mechanical behavior. To simulate the frequency responses of the resonators (arch and T-shaped beams) under electrothermal actuations and to take into account the various physical domains, various solvers have been utilized, which include the Solid Mechanics, Electric Currents, and Heat Transfer interfaces domains. Specific materials are selected and assigned to each domain. For the Solid Mechanics interface, the pads of the flexure beams and one side of the microbeams are set with a fixed constraint. For the Electric Currents, an electric potential is applied on one or both of the pads of the flexure beams (A and B) while the end of the arch beam is connected to ground (D). For the Heat Transfer, the thermal boundaries are set at ambient temperature at the bottom of the pads, and the rest of the structure is set to a convective heat boundary condition, where the heat flux option is used for an external natural convection with air as an external fluid and a vertical wall of height 1 m. Tetrahedral elements are used as the element type to mesh the structure. The simulation results of the resonance frequencies in the device are shown in Fig. 2 for the two actuation cases (BV^- and BV^+).

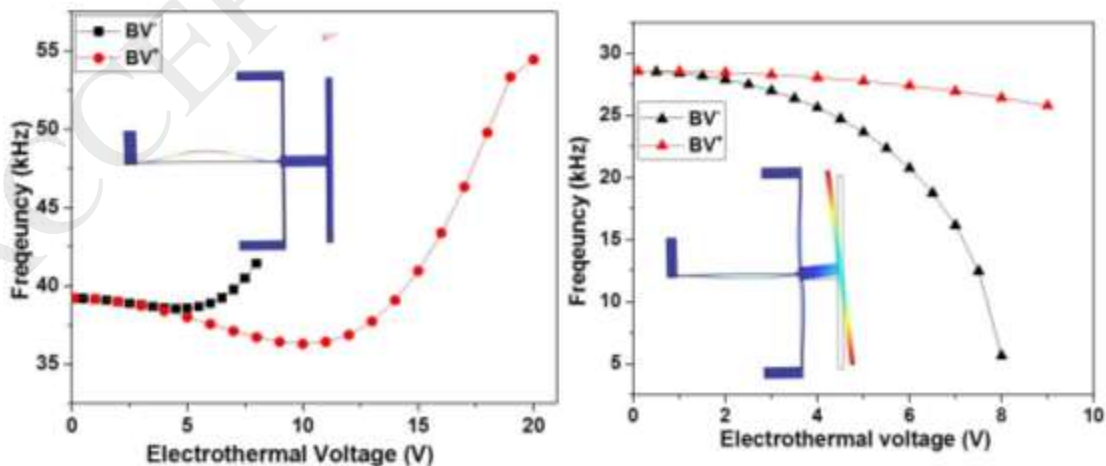

ACCEPTED MANUSCRIPT

(a) (b)

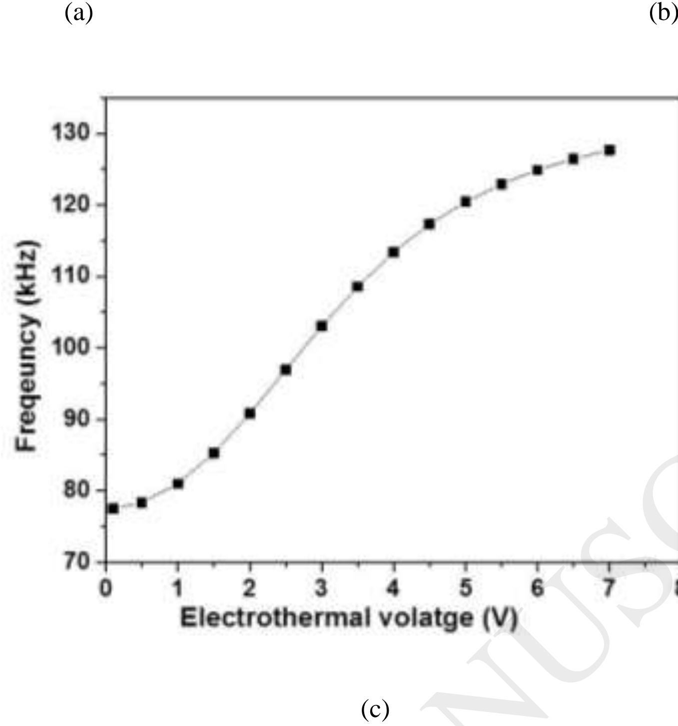

(c)

Fig. 2: The simulated change in the resonance frequency (a) of the arch beam and (b) the T-shaped beam for BV^- and BV^+. BV^- refers to powering the flexure beams by connecting Pad A with V^+ and Pad B with V^-, and Pad D to Ground (G). For BV^+ the pads A and B are powered by connecting them to the same voltage source V^+ and Pad D to ground. (c) The variation of the first resonance frequency of a clamped-clamped arch as varying the electrothermal voltage.

As in Fig. 2 (a), it is observed that for the two cases, the electrothermal voltage leads to an initial decrease in the first resonance frequency of the arch beam until it reaches a critical point (5 V for BV^- and 10 V for BV^+), after which it increases. The resonance frequency of the T-shaped beam on the other hand shows continuous decrease, Fig. 2 (b). A wider tunability range in the resonance frequency of the T-shaped beam is shown for BV^-. This shows the capability of shifting and choosing the operating frequency range upon demand.

In our previous work, we showed that when subjecting a clamped-clamped arch microbeam of high initial rise (b_0 >2.5 μm) to a compressive axial load through electrothermal actuation, increasing the compressive axial loads leads to increasing its first resonance frequency [30]. In order to gain deeper understanding of the influence of a pure axial load on the arch beam of this study; another simulation is conducted on a similar arch; however is made to be clamped-clamped so that we eliminate the effect of axial deformation at the anchor and focus only on the effect of the axial load. Fig. 2 (c) shows that, unlike Fig. 2(a) of the clamped-guided arch, the resonance frequency increases continuously. This confirms that the observed initial decrease in the resonance frequency of the arch in Fig. 2 (a) is due to the conditions at the guided boundary; particulary the axial (x) displacement of the guided part upon deforming the flexure beams.

ACCEPTED MANUSCRIPT

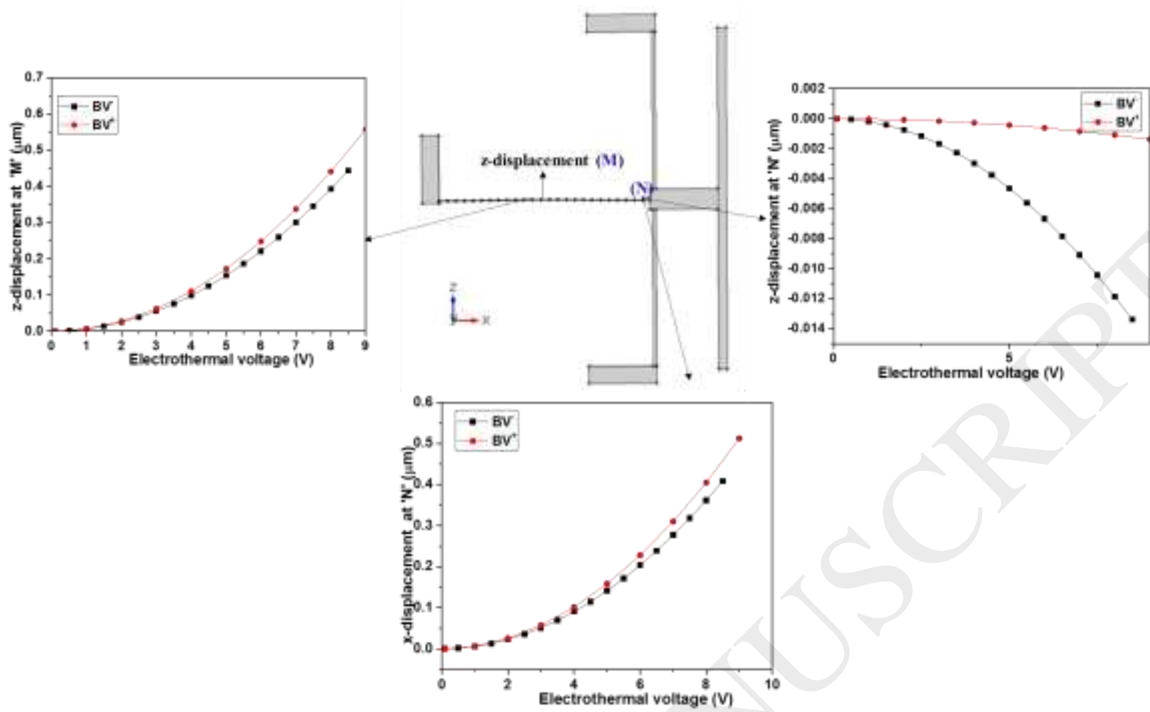

(a)

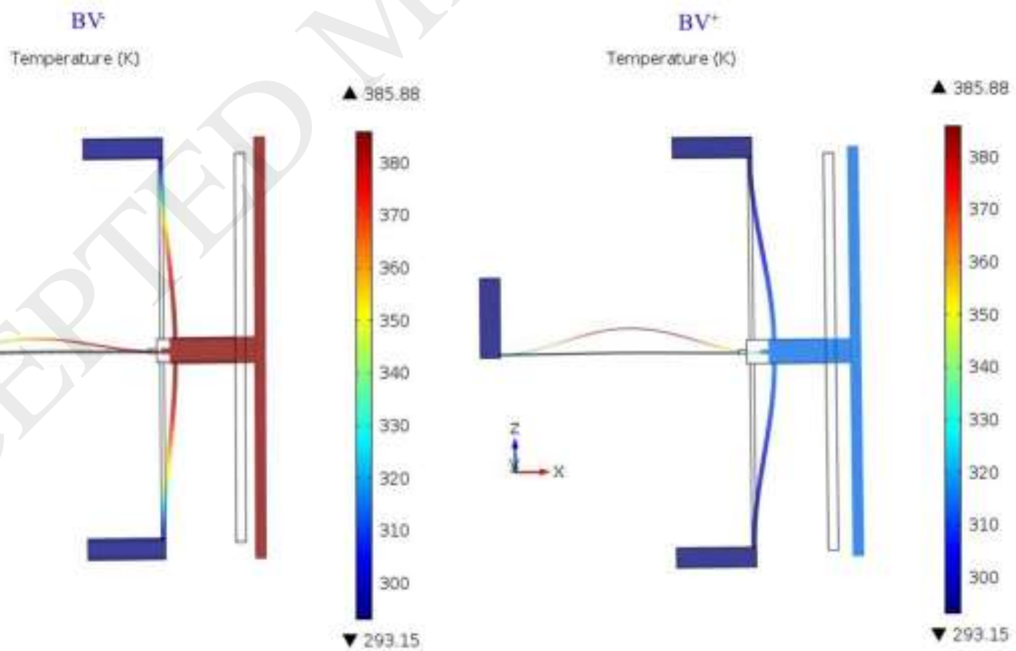

(b)

Fig. 3: FE simulations showing the mid-point z-deformation (point "M") of the arch, and the z and x-deformations at the guided end (point "N") as a function of electrothermal voltage for the two loading cases. (b) Temperature distribution in Kelvin for the two loading cases at an electrothermal voltage of 4 V.

ACCEPTED MANUSCRIPT

Simulation results of the z- deformation of the mid-point of the arch and at the guided end are shown in Fig. 3(a) for the two loading cases. Also this figure shows the axial displacement at the guided end. It is observed that for the two cases, the electrothermal voltage leads to an increase of the z-displacement and the x-displacement at the mid-point (M) and the guided end (N) at the same time. It can be observed also from the displacement curve that the z-displacement of the middle of the arch beam and the x-displacement on its guided end follows the same trend at low electrothermal voltages until it reaches 3 V for BV^- and 6 V for BV^+. Hence, it is concluded that the arch beam is influenced by both a tensile axial load from the axial displacement at the guided end and a compressive load from the electrothermal heating of the arch itself. The z-displacement of the arch is higher in BV^-than BV^+, which clarifies that the critical point of $BV^-$is too much lower than the BV^+. From the temperature distribution of the device, Fig. 3(b), the simulation result of BV^-shows a maximum temperature at the guided beam of 385.4 K while BV^+ shows a maximum temperature at the mid-point of the arch of 387.3 K at electrothermal voltage of 4 V.

Furthermore, the proposed design allows bi-directional movement of the arch beam in the x-axis. When an actuation voltage is applied between the compressive (tensile) electrode and the T-shaped beam, an axial compressive (tensile) stress is generated within the arch beam, Fig. 1. The details of the simulation method have been explained in [24]. Fig. 4 (a) shows finite element results of the resonance frequency for the first mode of the arch and the rotation mode of the T-shaped beam with varying compressive axial loads. It shows that the resonance frequency of the arch beam decreases when the electrostatic voltage increases due to the increase in the induced compressive load. For the T-shaped beam, it can be observed from Fig. 4 that the resonance frequency decreases. One can note here that for an axial compressive load, the frequency response of the arch beam is influenced by two mechanisms: the increase in stiffness of the arch due to the increase in its curvature and the decrease in the axial stress due to the axial compressive load. However, the results in Fig. 4(a) show that the stiffness effect of the arch beam dominates the reduction in its axial stress due to the decrease in curvature, and thus results in decreasing the resonance frequency.

ACCEPTED MANUSCRIPT

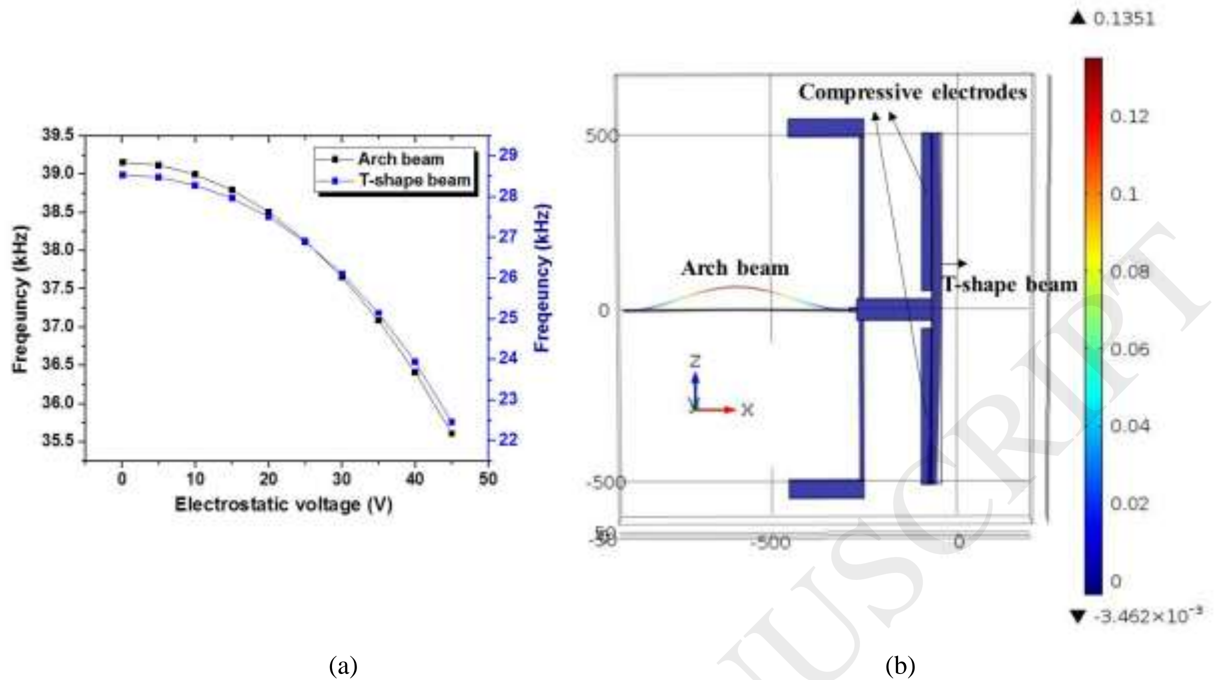

(a) (b)

Fig. 4: (a) The simulated change in the resonance frequency with the electrostatic compressive axial load for the first mode of the arch beam and the rotational mode of the T-shaped beam. (b) The static deformation (in μm) of the device at electrostatic voltage 25 V.

Next, a parametric study using FEM is performed on the arch beam to investigate the influence of the main geometrical parameters of the structure, mainly the initial rise b_0 and the width h, Fig. 5. It is observed that when b_0 decreases, the frequency range after the critical point increases, Fig 5(a). One notes here that the initial rise does not have any effect on the frequency variation of the T-shaped beam, Fig 5(b). Figs. 5(c) and 5(d) show the effect of h while fixing b_0 at 0 (straight beam). We found that for a thicker straight beam, the resonance frequency is almost constant until 10 V, after which it increases. The results also indicate that the frequency and the critical thermal voltage of the T-shaped beam, leading to its collapse, can be reduced by increasing the width of the arch beam, Fig. 5(d). This can be explained by the fact that the current passing through the flexure beams and the axial (x)-displacement of the guided part are higher in the case of the thicker straight beam.

ACCEPTED MANUSCRIPT

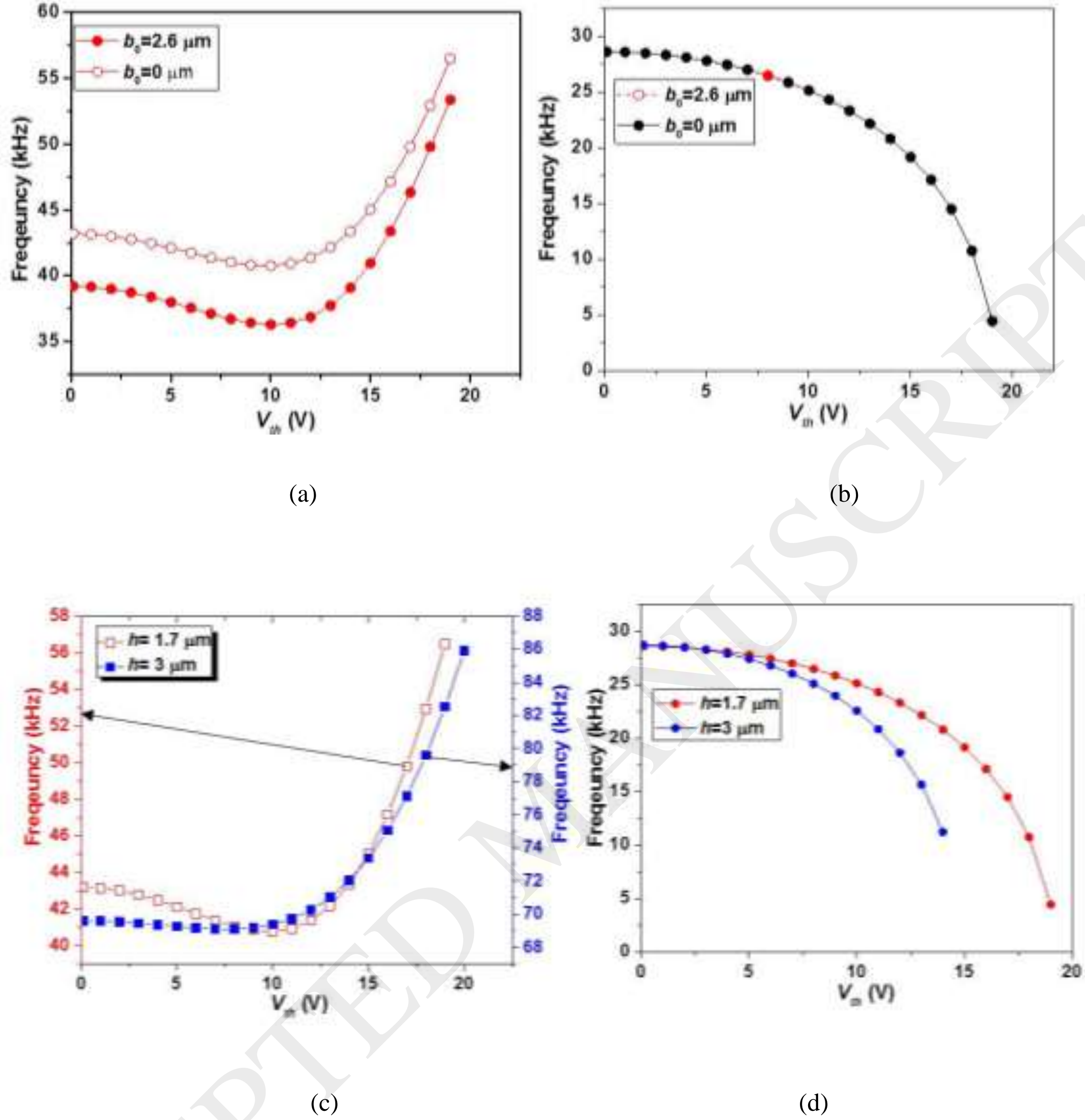

Fig. 5: The simulated fundamental resonance frequency of the arch and T-shaped beams for BV+, as varying V_{th}. Effect of b_0 at h= 1.7 µm on (a) arch beam and (b) T-shaped beam. Effect of h at b_0 = 0 µm on (c) arch beam and (d) T-shaped beam.

Figure 6 shows a FEM investigation of the effect of the electrothermal actuation on the natural frequency of the third mode of the straight beam (at h = 3 µm). The results demonstrate that the resonance frequency decreases as increasing the electrothermal voltage. In this case, the maximum percentage change in the resonance frequency is estimated to be 40 %.

ACCEPTED MANUSCRIPT

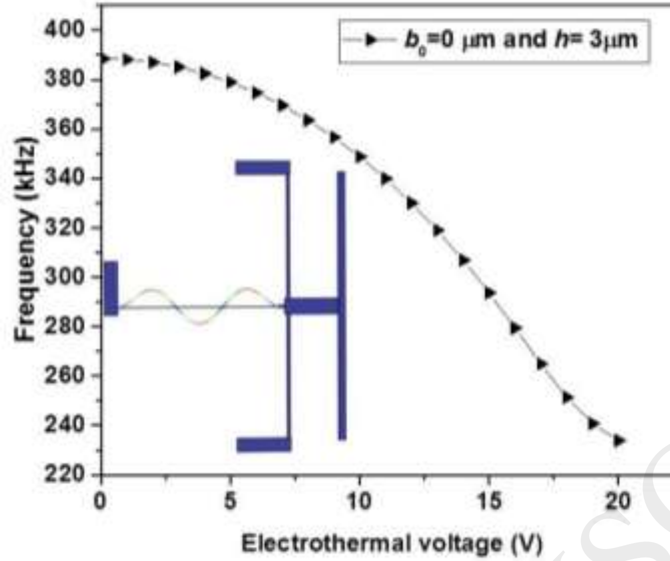

Fig. 6: The simulated change in the resonance frequency for the third mode (inset) of the straight beam.

4. Experimental results and discussions

To experimentally characterize and investigate the frequency response of the arch and the T-shaped beam, we utilized a Micro System Analyzer (MSA-500) from Polytec with an in-plane dynamic measurement system using a stroboscopic video microscopy. While varying the electrothermal voltage on the pads of the flexure beams, we measured the resonance frequencies of the microbeams using the ring-down measurement and the fast Fourier transform (FFT), where a sudden DC electrostatic load is applied on the arch beam then is removed to allow the microbeam to vibrate freely (ring down) until the motion dies out. Fig. 7(a) shows arch beam frequency response for the two cases under electrothermal actuation. In agreement with the finite element simulations, the experimental results show that the resonance frequency of BV^- decreases until reaching the critical point (5V) while the frequency response of BV^+ decreases continuously. Next, we combined the electrothermal actuation with the electrostatic force. We applied a compressive voltage (V_C) between the T-shaped beam and the stationary electrode, and then we varied the electrothermal voltage. Fig.7 (b) shows the instability threshold of the T-shaped structure, which can be understood as a function of two parameters; the thermal voltage and the applied electrostatic voltage from the side. The higher electrothermal voltage is, the lower the electrostatic voltage that leads to the collapse of the structure. Fig. 7(c) shows the first resonance frequency of the microbeam versus the electrothermal actuation for an electrostatic voltages of 25V and 35V, respectively. These values of DC bias are chosen arbitrarily; however they need to stay sufficiently below the pull-in voltage, which is estimated around 75 V. It can be observed that adding an electrostatic voltage leads to an increase of the axial load in the arch beam and to a change in the nature of the tunability. We can see that, from the tunability results, the resonance frequency of the arch beam electrothermally actuated or electrothermally and electrostatic actuated (25 V or 35 V) follows different trend until 8 V. After 8 V the three curves have the same values of resonance frequency.

ACCEPTED MANUSCRIPT

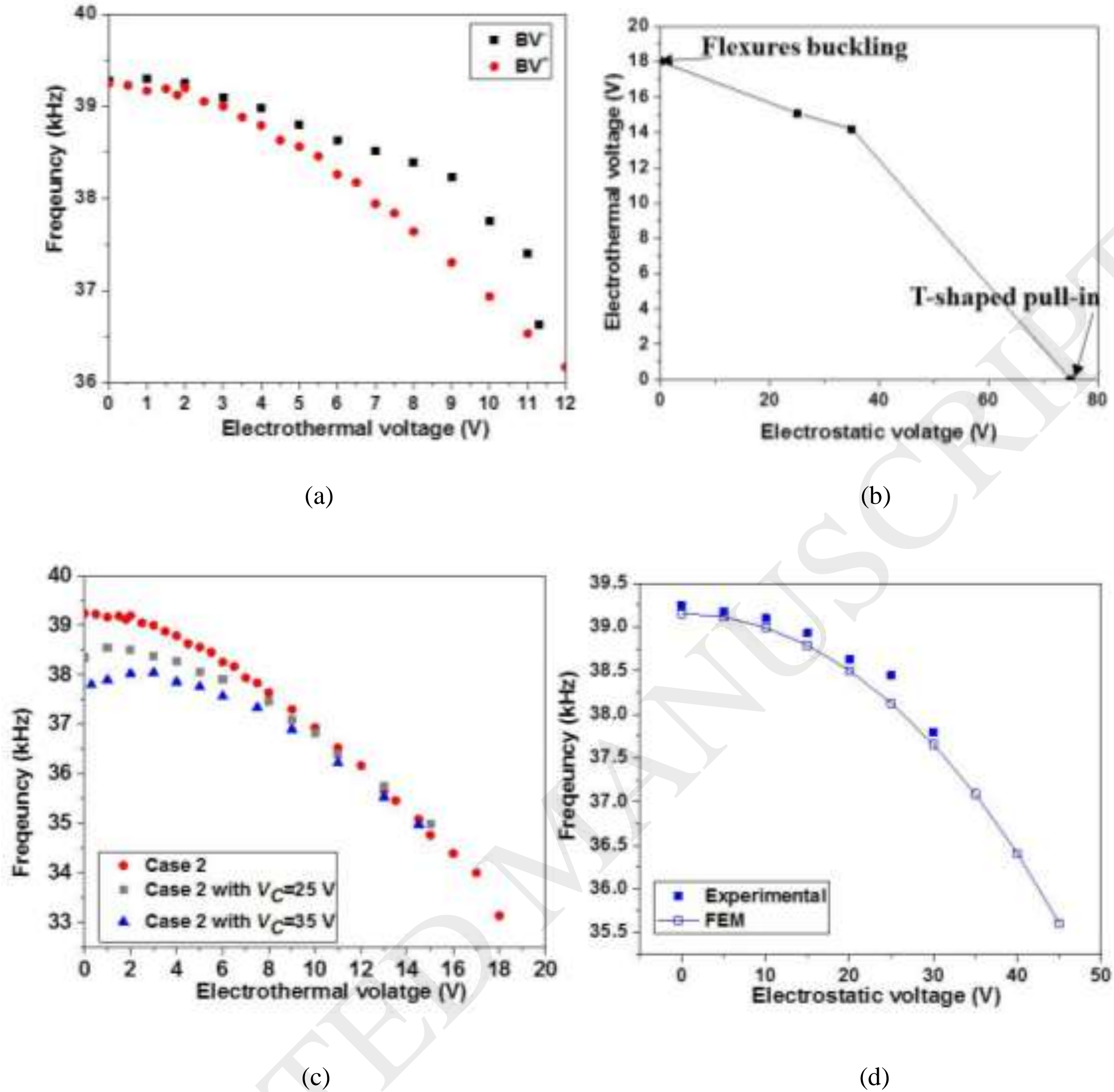

Fig. 7: (a) The measured change in the resonance frequency of the arch beam with electrothermal actuation for the two loading cases. (b) The measured instability threshold of the T-shaped structure. (c) The first resonance frequency of the microbeam versus electrothermal actuation for electrostatic compressive polarization voltages of 25 V and 35 V. (d) Measurements and FE simulations of the resonance frequency tuning with the compressive axial load V_C.

Fig. 7(d) shows the measurements of the resonance frequency for the first mode of the arch beam with varying compressive axial load. It shows that the resonance frequency of the arch decreases with the increase of the electrostatic voltage (V_C). A good agreement is shown among the finite element and experimental results.

5. Application: 1:2 DEMUX logic device

In this section, we demonstrate one of the potential applications of the studied device to perform a 1:2 DEMUX logic, which is commonly used as essential building block of many combinational logic circuits. A digital DEMUX

ACCEPTED MANUSCRIPT

can select the binary input to send it to parallel data signal at the output lines, it is also known as data distributor. Fig. 8 shows a 1:2 DEMUX schematic diagram, logic diagram, and truth table that involve one input, one select input, and two outputs.

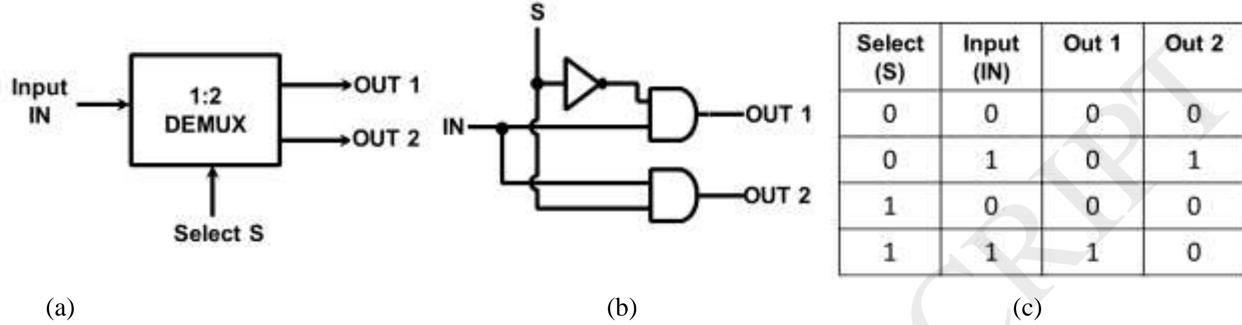

Select (S)	Input (IN)	Out 1	Out 2
0	0	0	0
0	1	0	1
1	0	0	0
1	1	1	0

(a) (b) (c)

Fig. 8: 1:2 DEMUX: (a) schematic diagram, (b) circuit diagram, (c) truth table.

To perform this logic device, the tunablity of both modes of the arch and T-shaped beams are experimentally obtained using a network analyzer (E5071C) and the setup shown in Fig. 9 (a). The lower electrode of the arch beam and one of the compressive electrodes of the T-shaped beam are used as the driving electrodes to excite the structure into the required mode of vibration. The arch and the T-shaped beams are excited by an AC actuation signal from the network analyzer and then superimposed with a DC voltage to their driving electrodes. The output current induced at the sense electrodes, upper electrode for the arch beam and the tensile electrode for the T-shaped beam, are connected to a low-noise amplifier (LNA) with its output coupled to the network analyzer input port for S_{21} transmission measurement. The two flexure beams are used as the selective (S) and they are electrothermally actuated to control the resonance frequencies of the arch beam (Output 1) and the T-shaped beam (Output 2). The second compressive electrode is used as the input (IN). For the arch beam (T-shaped beam) is biased with DC of 40V (15 V) and superimposed with an AC signal of 20mV (RMS) at room temperature and pressure of 2 Torr. The high motional current of a capacitively sensed resonator is taken as output HIGH at resonance. Off resonance, the low state/output, and hence motional current, is taken as LOW. Switch ON (OFF) condition represents logic 1(0) state of Selective input (S) and input (IN). The measured frequency response of the arch beam for the two cases is shown in Fig. 9 (b). As shown in this figure, the state of selective S is 0(1) for V_{th}= 0 V (3 V for the BV^{+}) while the state of input IN is 0(1) for V_C= 0 V (15 V), Fig. 9(c). Also Fig. 9 (c) shows that the ON states of S and IN (S=1 and IN=1) for V_{th}= 3 V and V_C= 15 V.

ACCEPTED MANUSCRIPT

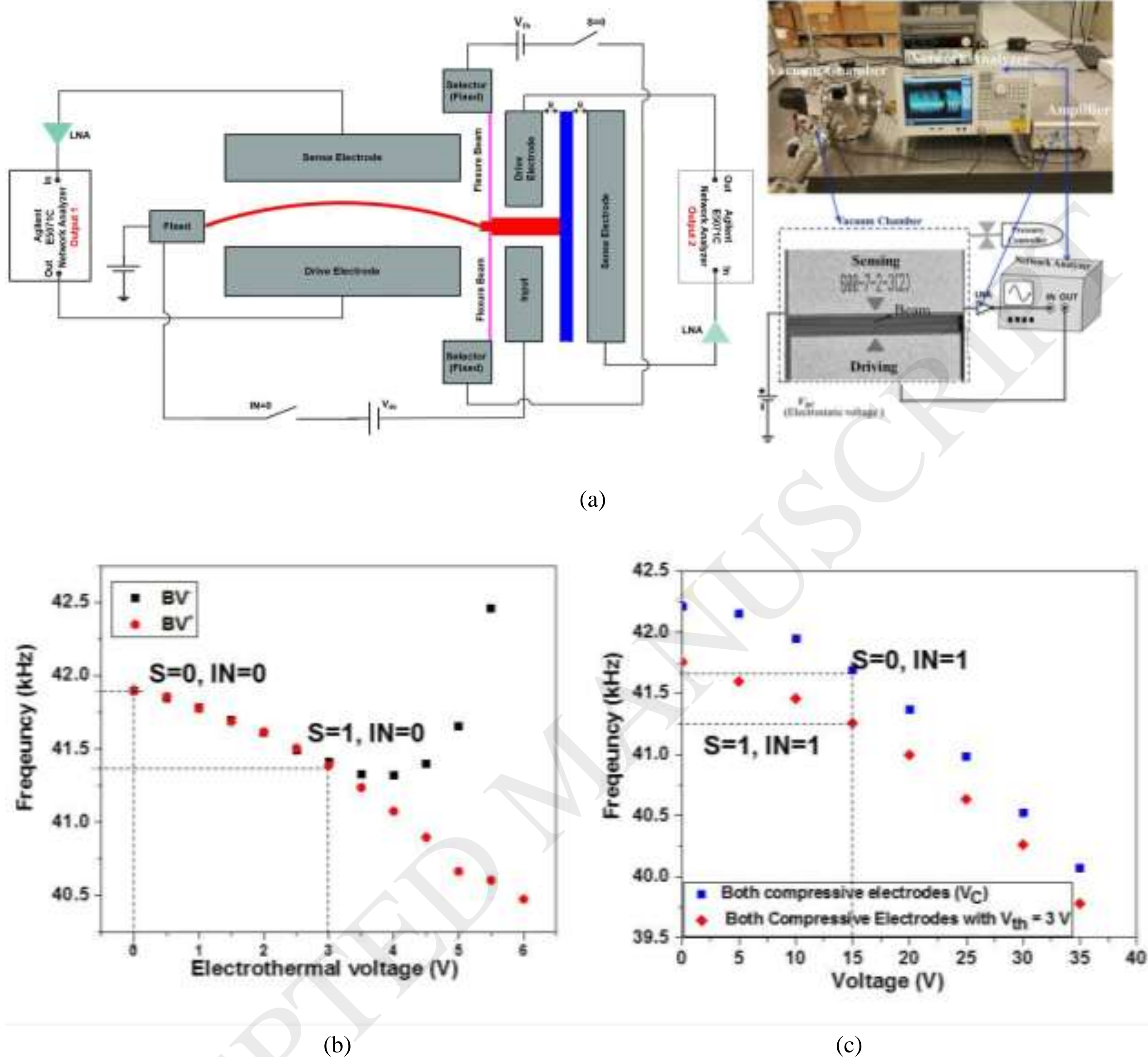

(a)

(b) (c)

Fig. 9: (a) A schematic and a photograph of the electrical experimental setup of the device. Measurement of the resonance frequency variation of arch beam (b) for the two cases (the electrothermal selective input is active for BV^+) and (c) under compressive electrostatic actuation (the input IN is active) and under electrostatic and electrothermal actuation with V_{th}= 3 V (the selective input and input are active).

Fig. 10 shows the measured S_{21} transmissions for the arch beam and the T-shaped beam. It indicates resonances frequencies for the arch beam and the T-shaped beam, respectively, around f_0 = 41.986 kHz and f_0 =24.036 kHz for (V_{th}=0 V, V_C=0 V (for one electrode)), $f_{0,1}$ = 41.63 kHz and $f_{0,1}$=23.099 kHz for (V_{th}=0 V, V_C=15 V), $f_{1,0}$ = 41.155 kHz and $f_{1,0}$ =22.06 kHz (V_{th}=3 V, V_C=0 V), and $f_{1,1}$ = 40.617 kHz and $f_{1,1}$ =21.424 kHz (V_{th}=3 V, V_C=15 V). The quality factors (Q) of the arch and T-shaped beams are estimated around 550 and 150, respectively. Based on Fig. 10, the signal-noise ratio SNR is estimated around 25 dB. The magenta and the black curves (the red and the blue) represent the case of select input S=0 (S=1) line. Now, for S=0 and IN=1, the T-shaped beam is on resonance

ACCEPTED MANUSCRIPT

state at 23.099 kHz, and, hence, the output 2 will show HIGH (1). On the other hand, for S=1 and IN= 1, the output 1 will show HIGH (1) state at 40.617 kHz. For the other cases (S=0, IN=0) and (S=1, IN=0), the two outputs will show LOW (0) state. The time responses showing the logic outputs for IN=1 are shown in Fig. 11. As shown in this figure and for example in the case of the off state (0) for the selected S=0, the outputs of the arch and the T-shaped beams, shown in red, are 0 and 1, respectively. Hence, the proposed circuit indeed shows the correct DEMUX outputs.

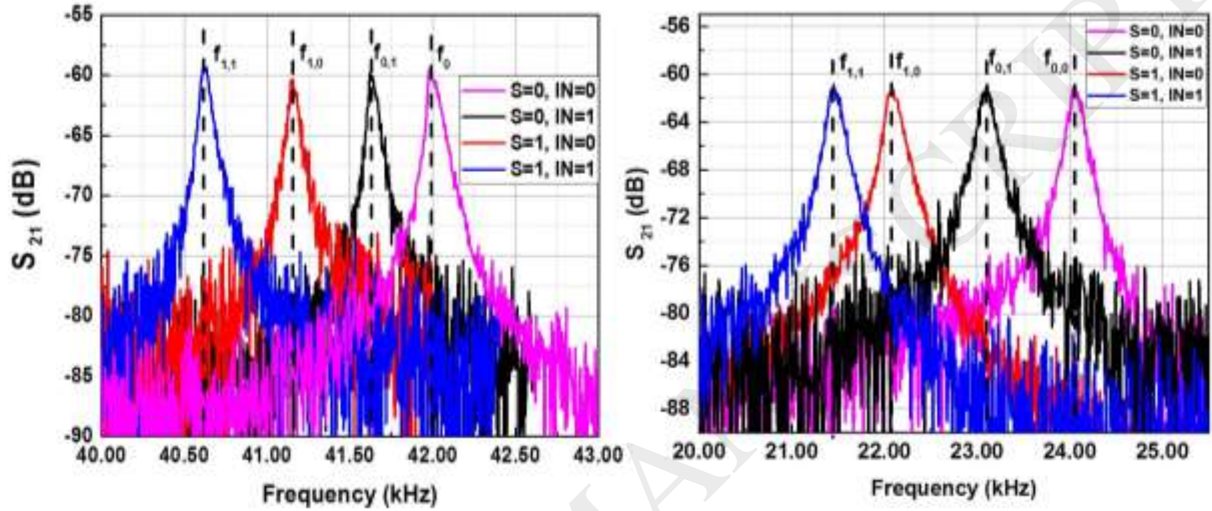

(a) Output 1 (b) Output 2

Fig. 10: Frequency responses of (a) the arch beam and (b) the T-shaped beam for the logic input and select input conditions of (0,0), (0,1), (1,0), and (1,1), shown in magenta, black, red, and blue, respectively.

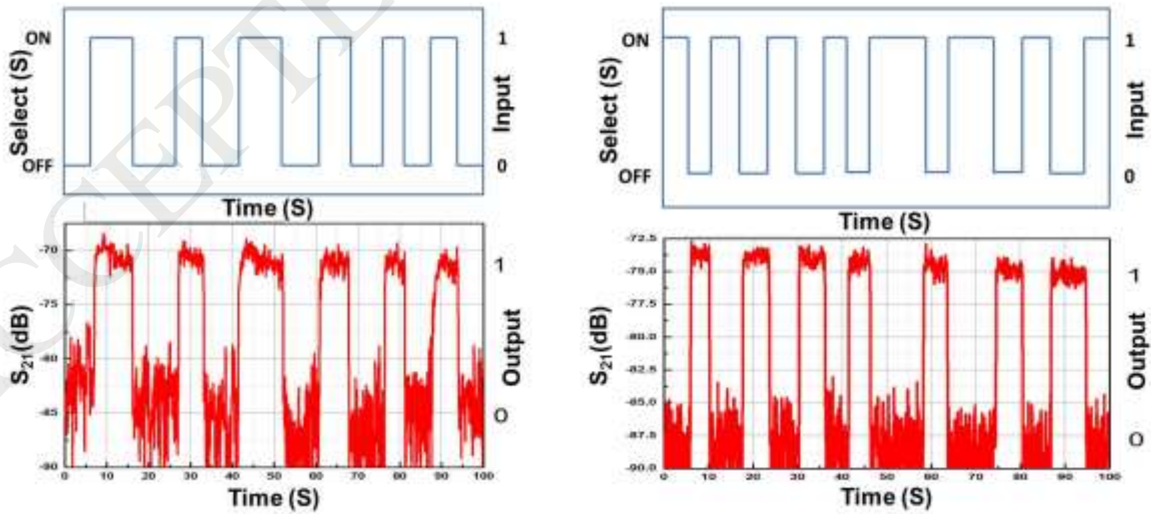

(a) Output 1 (b) Output 2

Fig. 11: Time response at IN=1 from (a) Output 1 and (b) Output 2.

ACCEPTED MANUSCRIPT

6. Performance evaluation of 1:2 DEMUX logic device

The performance of the proposed logic device can be evaluated based on two criteria: switching speed (f0/Q) and switching power consumption [31]. Based on the resonance frequencies and quality factors of the two beams, the switching speed is estimated to be 76 Hz and 160 Hz, respectively. Thus, their switching time is found to be 13.16 ms and 6.25ms, respectively. The switching time can be improved by increasing the resonance frequency of the device by scaling down its dimensions and by operating the structure in higher order modes. The power consumption of the structure is estimated to be around 128 μJ and 63.53 μJ for the two beams. Compared to CMOS devices, the current structure shows higher power consumption. This can be resolved by also scaling down the dimensions of the device. However, the advantage of this structure is that it can offer various read-out possibilities and multiple input ports, which can lead to complex device functionalities that can reduce the total number of devices required to achieve deep logic functions, and hence eventually mad lead to lower power consumption.

7. Conclusions

This paper presented MEMS resonators with multiple electrical input and output possibilities. The design relies on in-plane arch clamped-guided microbeam attached to another T-shaped beam from the side, in which the two beams are excited electrostatically. In addition, the design is provided with two electrothermally actuated flexures beams that are used for tuning the resonance frequencies of the beams. Through theoretical and experimental investigations, we examined different ways of both sensing and actuation of two mechanically coupled resonators. We demonstrated that this configuration allows the realization of complex logic operations, such as a 1:2 DEMUX. The experimental results showed that this device can be reconfigured to enable different multifunctional and complex logic operations depending on the actuation ways and the combination of the logic inputs and the two logic outputs.

Acknowledgment

This publication is based upon work supported by the King Abdullah University of Science and Technology (KAUST) office of sponsored research OSR under Award No. OSR-2016-CRG5-3001.

8. References

[1] A.Z Hajjaj, N. Alcheikh, M.A.A. Hafiz, S. Ilyas, M.I. Younis, A scalable pressure sensor based on an electrothermally and electrostatically operated resonator. Applied Physics Letters, 111(2017), 223503.
[2] D. Kim, E. Lee, M. Cho, C. Kim, Y. Park, T. Kouh, Pressure-sensing based on photothermally coupled operation of micromechanical beam resonator. Applied Physics Letters, 102 (2013) 203502.
[3] Y. Kessler, S. Krylov, A. Liberzon, Flow sensing by buckling monitoring of electrothermally actuated double-clamped micro beams. Applied Physics Letters, 109(2016), 083503.
[4]A. Bouchaala, N. Jaber, O. Shekhah, V. Chernikova, M. Eddaoudi, M.I. Younis, A smart microelectromechanical sensor and switch triggered by gas. Applied Physics Letters, 109(2016), 013502.
[5] M. Hajhashemi, A. Amini, B. Bahreyni, A micromechanical bandpass filter with adjustable bandwidth and bidirectional control of centre frequency. Sensors and Actuators A: Physical, 187 (2012) 10-15.
[6] B. Charlot, W. Sun, K. Yamashita, H. Fujita, H. Toshiyoshi, Bistable nanowire for micromechanical memory. Journal of Micromechanics and Microengineering, 18 (2008) 045005.

ACCEPTED MANUSCRIPT

[7] M.A. Hafiz, S. Tella, N. Alcheikh, H. Fariborzi, M.I. Younis, Axially modulated arch resonator for logic and memory applications. Mechatronics, 2018.
[8] F.K. Chowdhury, D. Saab, M. Tabib-Azar, Single-device “XOR” and “AND” gates for high speed, very low power LSI mechanical processors. Sensors and Actuators A: Physical, 188 (2012),481-8.
[9] N. Krakover, B.R. Ilic, S. Krylov, Displacement sensing based on resonant frequency monitoring of electrostatically actuated curved micro beams. Journal of Micromechanics and Microengineering, 26 (2016) ,115006.
[10] C. M. Ho, Y.C. Tai, Y.C, Micro-electro-mechanical-systems (MEMS) and fluid flows. Annual Review of Fluid Mechanics, 30(1998), 579-612.
[11] U. Y.H. Wang, C.P. Chen, C.M. Chang, C.P. Lin, C.H. Lin, L.M. Fu and C.Y. Lee, MEMS-based gas flow sensors. Microfluidics and nanofluidics, 6(2009), 333.
[12] R.R. Syms, Electrothermal frequency tuning of folded and coupled vibrating micromechanical resonators. Journal of microelectromechanical systems, 7(1998), 164-171.
[13] J.R. Liu, S.C. Lu, C.P. Tsai, W.C. Li, A CMOS-MEMS Clamped-Clamped Beam Displacement Amplifier for Resonant Switch Applications. Journal of Micromechanics and Microengineering, 2018.
[14] B. Svilicic, E. Mastropaolo, B. Flynn, R. Cheung, 2012. Electrothermally actuated and piezoelectrically sensed silicon carbide tunable MEMS resonator. IEEE electron device letters, 33(2012),278-280.
[15] G. Zhang, V. Chu, J.P. Conde. Electrostatically actuated bilayer polyimide-based microresonators. Journal of Micromechanics and Microengineering, 17(2007),797.
[16] N. Alcheikh, L. Kosuru, N. Jaber, M. Bellaredj, Mohammad I. Younis, Influence of squeeze film damping on the higher-order modes of clamped–clamped microbeams. Journal of Micromechanics and Microengineering 26 (2016), 065014.
[17] W. Zhang, J.E.Y. Lee, Characterization and modeling of electro-thermal frequency tuning in a mechanical resonator with integral crossbar heaters. Sensors and Actuators A: Physical, 202 (2013), 69-74.
[18] N. Alcheikh, A. Hajjaj, N. Jaber, M. Younis, Electrothermally actuated tunable clamped-guided resonant microbeams Mech. Syst. Signal Process., 98 (2018), 1069-1076
[19] N. Alcheikh, S.A. Tella, M. I. Younis. Adjustable static and dynamic actuation of clamped-guided beams using electrothermal axial loads Sensors and Actuators A: Physical, 273 (2018), pp. 19-29.
[20] T. Remtema, L. Lin, Active frequency tuning for micro resonators by localized thermal stressing effects. Sensors and Actuators A: Physical, 91(2001), pp.326-332.
[21] Y. Cha, H. You, Torsion Sensing based on Patterned Piezoelectric Beams. Smart Materials and Structures, 2018.
[22] B. Halg , On a micro-electro-mechanical nonvolatile memory cell. IEEE Transactions on Electron Devices, 37(1990),2230-2236.
[23] M.A. Hafiz, L. Kosuru, MI. Younis, Microelectromechanical reprogrammable logic device. Nature communications, 7(2016),11137.
[24] N. Alcheikh, A. Ramini, M. A. Hafiz, M.I. Younis, Tunable Clamped–Guided Arch Resonators Using Electrostatically Induced Axial Loads. Micromachines, 8(2017),14.
[25] I. Mahboob, E. Flurin, K. Nishiguchi, A. Fujiwara, H. Yamaguchi, Interconnect-free parallel logic circuits in a single mechanical resonator. Nature communications, 2 (2011), 198.
[26] H. Noh, S. B. Shim, M. Jung, Z. G. Khim, and J. Kim, A mechanical memory with a dc modulation of nonlinear resonance. Applied Physics Letters , 97(2010), 033116.
[27] A.Yao, T. Hikihara, Logic-memory device of a mechanical resonator. Applied Physics Letters. 12 (2014),123104.
[28] M.A. Hafiz, L. Kosuru, M.I. Younis, H. Fabrozi, 2: 1 MUX based on multiple MEMS resonators. Procedia Engineering, 168 (2016), pp.1642-1645.
[29] J.S Wenzler, T. Dunn T, T. Toffoli , P. Mohanty, A nanomechanical Fredkin gate. Nano letters, 14(2013), 89-93.
[30] A.Z Hajjaj, A. Ramini, N. Alcheikh, M.I. Younis, Electrothermally tunable arch resonator. Journal of Microelectromechanical Systems, 26(2017), 837-845.

[31] S.A. Tella, N. Alcheikh, M.I. Younis, A single MEMS resonator for reconfigurable multifunctional logic gates. Journal of Micromechanics and Microengineering, 28(2018), 095002.

ACCEPTED MANUSCRIPT

Nouha Alcheikh was born in 1984. She received her MS degree in electronics from the Polytechnic National Institute of Grenoble in 2007 and her PhD degree in RF MEMS from Grenoble University, France in 2011. From 2011 to 2014, she was as a Post-Doctoral fellow working on Force Sensors and Energy Harvesting at CEA-Leti/MINATEC Campus, Grenoble (France) and at IMS, Bordeaux (France). Since 2015, she has been a Post-Doctoral Fellow at King Abdullah University of Science and Technology, Thuwal, Saudi Arabia where she is performing her research on MEMS Sensors and Actuators,

Sherif Tella Sherif Tella received his ND (National Diploma) in Mechanical Engineering from Yaba College of Technology, Nigeria in 2005 and B.Sc degree in Mechanical Engineering from Obafemi Awolowo University, Nigeria in 2010. Then, He was awarded with MSc. with Distinction in Mechatronics from University of Glasgow, Glasgow, UK in 2014. He is currently enrolled as PhD student in Mechanical Engineering in KAUST. His research interests include dynamics and control of linear and nonlinear systems in MEMS and NEMS devices with applications in logics, memory, filters etc. He was

Mohammad I. Younis received a Ph.D. degree in engineering mechanics from Virginia Tech in 2004. He is currently an Associate Professor of Mechanical Engineering with King Abdullah University of Science and Technology, Saudi Arabia. He serves as an Associate Editor of Nonlinear Dynamics, the Journal of Computational and Nonlinear Dynamics, and the Journal of Vibration and Control. He is a member of IEEE and the American Society of Mechanical Engineers ASME.

ACCEPTED MANUSCRIPT